METER-SIZED CRATERS AND BOULDERS AROUND LUNAR SOUTH POLE SHACKLETON AND NORTH POLE WHIPPLE CRATERS. O. Kawashima[1], T. Morota[1], M. Ohtake[2], and S. Kasahara[1], [1]The university of Tokyo, 7-3-1 Hongo, Bunkyo-ku, Tokyo, Japan (o.kawashima@eps.s.u-tokyo.ac.jp), [2]University of Aizu, Tsuruga, Ikki-machi Aizu-Wakamatsu, Fukushima, 965-8580, Japan.

Introduction: The existence of volatiles, especially hydrogen (or presumably H_2O ice), in the lunar polar regions has been supported by observations of LCROSS impact plumes [1] and other spacecraft remote sensing like neutron spectrometry [2–3], although negative reports also exist [4]. Interest in this topic has motivated a growing number of future scientific and technological lunar polar missions around polar craters, which host permanently shadowed regions [5–8]. In many polar missions, landing-site candidates are directly visible from the Earth, nearby the permanently shadowed regions, in sunlit areas, and on gentle slopes [8–12]. Besides, for the landing and exploration site selection, the spatial distributions and densities of craters and boulders are indispensable. For example, the spatial information of craters and boulders must be available on meter-sized scales (10 m at least) to determine the landing ellipses of rovers [13]. However, the number density and size frequency of craters and boulders around those candidate sites remains unknown.

This study provides size–frequency measurements of the meter-sized craters and boulders around the South pole Shackleton and the North pole Whipple. Based on our counting results, we assess the risk of landing-site candidates for future lunar polar exploration missions. Because the sizes of the smallest craters and boulders exceeds a few meters in our study, the sites should be refined by examining the higher resolution images (i.e., tens of centimeters) like close-up images of the site before landing, and images which are currently taken by Chandrayaan-2 [14].

Study regions and analyzed data: We chose a 900-km^2 square area containing the entire rim of the 21-km-diameter Shackleton crater centered on 89.6°S, 139.5°E and a 400-km^2 square area containing the entire rim of the 15-km-diameter Whipple crater centered on 89.2N°, 119.5°E (Figure 1). We manually counted the craters and boulders in the mosaic images (~1 m/pix) based on Lunar Reconnaissance Orbiter Camera/Narrow Angle Camera observation [15]. We used Digital Elevation Model from Lunar Orbiter Laser Altimeter [16] to analyze regional slope.

Results and Discussion: We identified 238,844 craters and 2,973 boulders around Shackleton crater, and 67,730 craters and 7,375 boulders around Whipple crater, respectively. The counting results are shown in Figures 2 and 3. The list of craters and boulders will be available on a website.

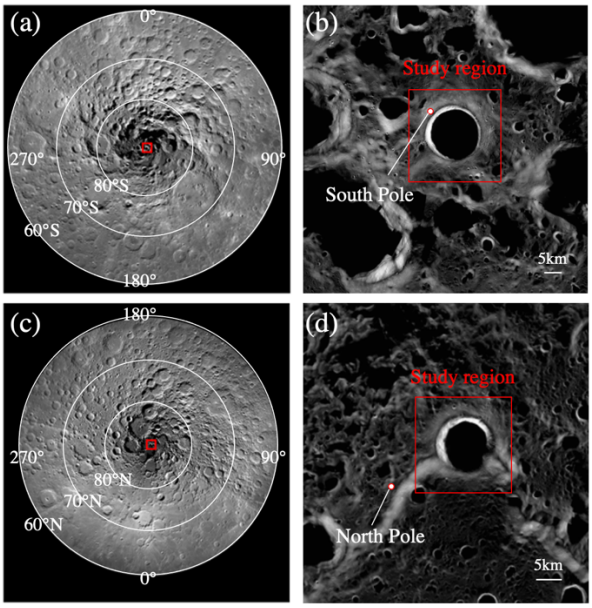

Figure 1. LROC/NAC mosaic images showing our study areas. (a) and (b) show the 30 km × 30 km square area containing Shackleton crater; (c) and (d) show the 20 km × 20 km square area containing Whipple crater. White circles in (b), (d) indicate the positions of the South and North pole. All images are taken from a map assembled by Arizona State University, downloaded from *Moon Trek* (Day and Law (2018)).

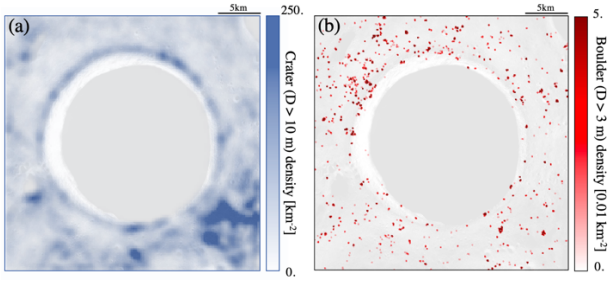

Figure 2. Number density maps of identified (a) small craters and (b) boulders around Shackleton crater.

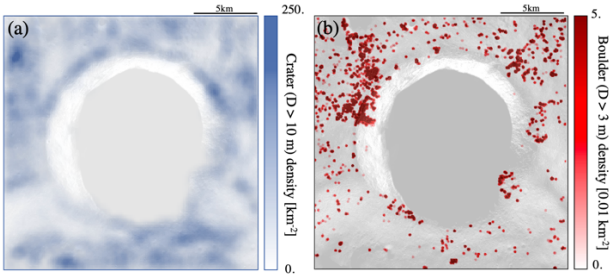

Figure 3. Number density maps of identified (a) small craters and (b) boulders around Whipple crater.

Using the crater areal density calculated in this study, we reassessed the candidate sites of future missions around Shackleton crater. For the site assessment, we also referred to the distance from permanently shadowed regions (including small ones dotted around Shackleton crater), areal slope steepness, and illumination conditions (Figure 4). We subdivided the study regions into 2 km×2 km units as shown in Figure 4 (a), evaluating the merits of each site. Finally we identified "A" in Figure 4 as a common point of low-crater density region (50 km^{-2} for craters >10 m in diameter), mild-slope region (<15 degree in average), persistently illuminated region (>50 % in one lunar year), and neighbor (< 5 km) of permanently shadowed region.

We focused on the region around "A". Figure 5 (a) shows the permanently shadowed regions [11] and the regions estimated to be bearing ice exposures [17]. Figure 5 (b) shows identified crater maps in "A", emphasizing a fresh crater which is densely populated with boulders.

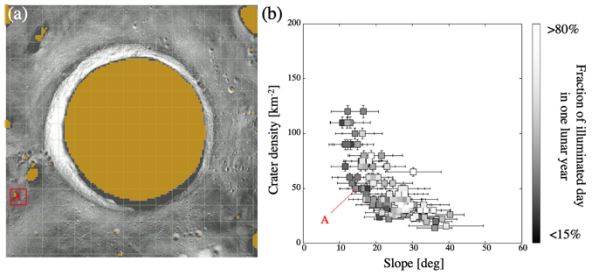

Figure 4. (a) A map showing analyzed subdivisions (2 km × 2 km square areas, separated by green lines). Red areas show permanently shadowed regions [11]. (b) Correlations between the average slope and the crater number density (>10 m in diameter) in each 2 km × 2 km unit in the Shackleton area. The grayscale color contour indicate the amounts of solar irradiation in each unit, estimated from illumination maps [11].

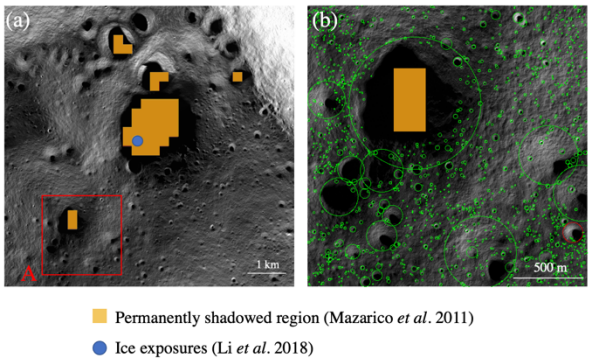

Figure 5. (a) A map around region "A", showing permanently shadowed regions [11] and ice exposures [17]. (b) Crater maps in region "A". Red circle shows a crater with high boulder density (~1000 km^{-2}).

In addition to the permanently shadowed regions, low-temperature subsurface area in sunlit regions is considered to be another prospective place for the water concentration [18–19]. As shown in Figure 6 (a), crater ejecta maps can be produced from the crater location map (i.e., Figure 5 (b)) using the empirical model of the ejecta thickness [20]. The crater ejecta map will be helpful to future regolith drilling and icy measurements [8].

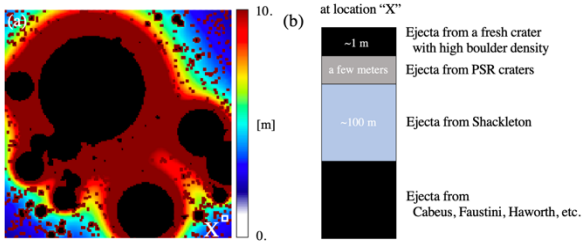

Figure 6. (a) Crater ejecta map produced from crater size and location map (Figure 5 (b)), using empirical model of the ejecta thickness [20]. (b) Vertical ejecta thickness model in region "X", shown in (a).

References: [1] Colaprete *et al.* (2010) *Science, 33, 6003,* 463–468. [2] Feldman *et al.* (1998) *Science, 281, 1496* [3] Mitrofanov *et al.* (2010) *Science, 330, 6003, 483–486* [4] Haruyama *et al.* (2009) *Science, 322, 5903*, 938–939 [5] Colaprete *et al.* (2019) *AGU Abstract #P34B-03* [6] Ohtake *et al.* (2021) *52nd LPSC Abstract #1840* [7] Smith *et al.* (2020) *IEEE Aerospace Conference, 1–10* [8] Ohtake *et al.* (2020) *51st LPSC Abstract #1830* [9] Gläser *et al.* (2014) *Icarus, 243, 78–90* [10] Mazarico *et al.* (2011) *Icarus, 211, 1066–1081* [11] Speyerer and Robinson (2013) *Icarus, 222, 122–136* [12] Inoue *et al.* (2020) *51st LPSC Abstract #1772* [13] Ueda *et al.* (2017) *26th ISSFD, ISTS-2017-D-053/ISSFD-2017-053* [14] Chowdhury *et al.* (2020) *Current Science, 118, 4, 560–565* [15] Day and Law (2018) *42nd COSPAR Scientific Assembly B3.1-11-18* [16] Smith *et al.* (2011) *Lunar Planet. Sci. XLII, 2350* [17] Li *et al.* (2018) *Proc. Natl. Acad. Sci. 115, 201802345* [18] Reiss *et al.* (2021) *J. Geo. Res.: Planets. 126, e2020JE006742* [19] Schorghofer and Taylor, (2007) *J. Geophys. Res. 112, E2010* [20] Pike (1974) *Earth Planet. Sci. Lett. 23, 265–274*